A 2-D Artificial Dielectric With $0 \leq n < 1$ for the Terahertz Region

Rajind Mendis, *Member, IEEE*, and Daniel M. Mittleman, *Senior Member, IEEE*

***Abstract*—We demonstrate a 2-D artificial dielectric medium suitable for the terahertz region by exploiting the characteristic frequency dependence in the phase velocity of the lowest order transverse-electric (TE_1) mode of the parallel-plate waveguide (PPWG). This artificial medium exhibits a plasma-like behavior having a frequency-dependent refractive index that varies between zero and unity. Using this medium, we demonstrate the optical phenomena of total internal reflection and Brewster's effect, and also demonstrate a convergent PPWG-lens.**

***Index Terms*—Artificial dielectrics, dispersive media, parallel-plate waveguides (PPWGs), terahertz.**

I. Introduction

THE parallel-plate waveguide (PPWG) has been extensively investigated for fundamental and applied research in the terahertz region of the electromagnetic spectrum, exploiting the many advantages of its dominant transverse-electromagnetic (TEM) mode [1]–[17]. However, until recently [18], [19], the lowest order transverse-electric (TE_1) mode of the PPWG was virtually unexplored in the terahertz region mainly due to the "undesirable" dispersive effect caused by its inherent cutoff. In this study, we demonstrate that this dispersive effect can be gainfully exploited to convert a PPWG structure into an artificial dielectric medium with unique properties. We demonstrate several manifestations of the properties of this medium, all relying on the fact that its effective refractive index is less than one.

The dispersion of the TE_1 mode in a PPWG is evident from the dramatic frequency dependence in the phase velocity (v_p) near the mode's cutoff. For an air-filled PPWG, v_p increases from c to infinity as the operating frequency approaches cutoff. Using the well-known expression for v_p [20], we can derive an effective refractive index as

$$n = \frac{c}{v_p} = \sqrt{1 - \left(\frac{f_c}{f}\right)^2} \tag{1}$$

where $f_c = c/(2b)$ is the cutoff frequency, and b is the plate separation. This implies that n varies from a value close to unity at high frequencies, to zero as the frequency reaches cutoff. Therefore, a wave propagating in the TE_1 mode inside the PPWG experiences a medium with $0 \leq n < 1$: a 2-D artificial dielectric medium.

We should emphasize that although this is a novel concept in the terahertz region, this plasma-like behavior of the PPWG has been recognized more than half a century ago in the microwave region [21]–[25]. However, since the wavelengths in the microwave region are typically a few centimeters, compared to the sub-millimeter wavelengths in the terahertz region, the PPWG structures employed in the microwave region were relatively large and bulky.

This artificial-dielectric effect provides an ideal platform to demonstrate the merging of the microwave and optical regions via the terahertz region, where microwave waveguide concepts can be used to demonstrate fundamental optical phenomena such as *total internal reflection* (TIR) and *Brewster's effect*. We experimentally demonstrate these optical effects using various PPWG configurations operating in the TE_1 mode, and also demonstrate a convergent PPWG-lens with a strong focusing power suitable for terahertz radiation.

II. Initial Experiment

To confirm the frequency-dependent behavior of the refractive index, our initial experiment incorporated a 45° PPWG-prism fabricated using two polished triangular aluminum plates [see Fig. 1(a)]. As shown, a beam of broadband terahertz pulses [inset of Fig. 1(d)] was focused to a 10-mm ($1/e$ amplitude) diameter and directly coupled into the prism at normal incidence with the electric field polarized parallel to the plate surfaces. The beam propagates via the single TE_1 mode through the prism, and encounters the exit face at an angle of 45°. At this face, the wave experiences a sudden change in index, and in keeping with Snell's law, changes its direction. In fact, the output beam bends towards the normal since it is traveling from a medium of low index ($n < 1$) to free space. This dispersive effect is opposite to that observed in a conventional dielectric, where the wave travels from a high-index ($n > 1$) medium to free space, bending away from the normal. The refraction is highly frequency dependent, as the low-frequency components (closer to f_c) refract more than the high-frequency components.

We detect the output signal by positioning a fiber-coupled terahertz receiver along an arc, equidistant from the axial exit point. The detected terahertz signals at various angular positions (θ) are shown in Fig. 1(b) with their corresponding spectra in Fig. 1(c) for $b = 1$ mm (corresponding to $f_c = 0.15$ THz). The time-domain waveforms exhibit a negative chirp, with high-frequency components arriving earlier in time, characteristic of

Manuscript received September 14, 2009; accepted February 04, 2010. Date of publication June 07, 2010; date of current version July 14, 2010. This work was supported in part by the U.S. National Science Foundation (NSF) and by the Air Force Research Laboratory under the CONTACT Program.

The authors are with the Department of Electrical and Computer Engineering, Rice University, Houston, TX 77005 USA (e-mail: rajind@rice.edu; daniel@rice.edu).

Color versions of one or more of the figures in this paper are available online at http://ieeexplore.ieee.org.

Digital Object Identifier 10.1109/TMTT.2010.2050386

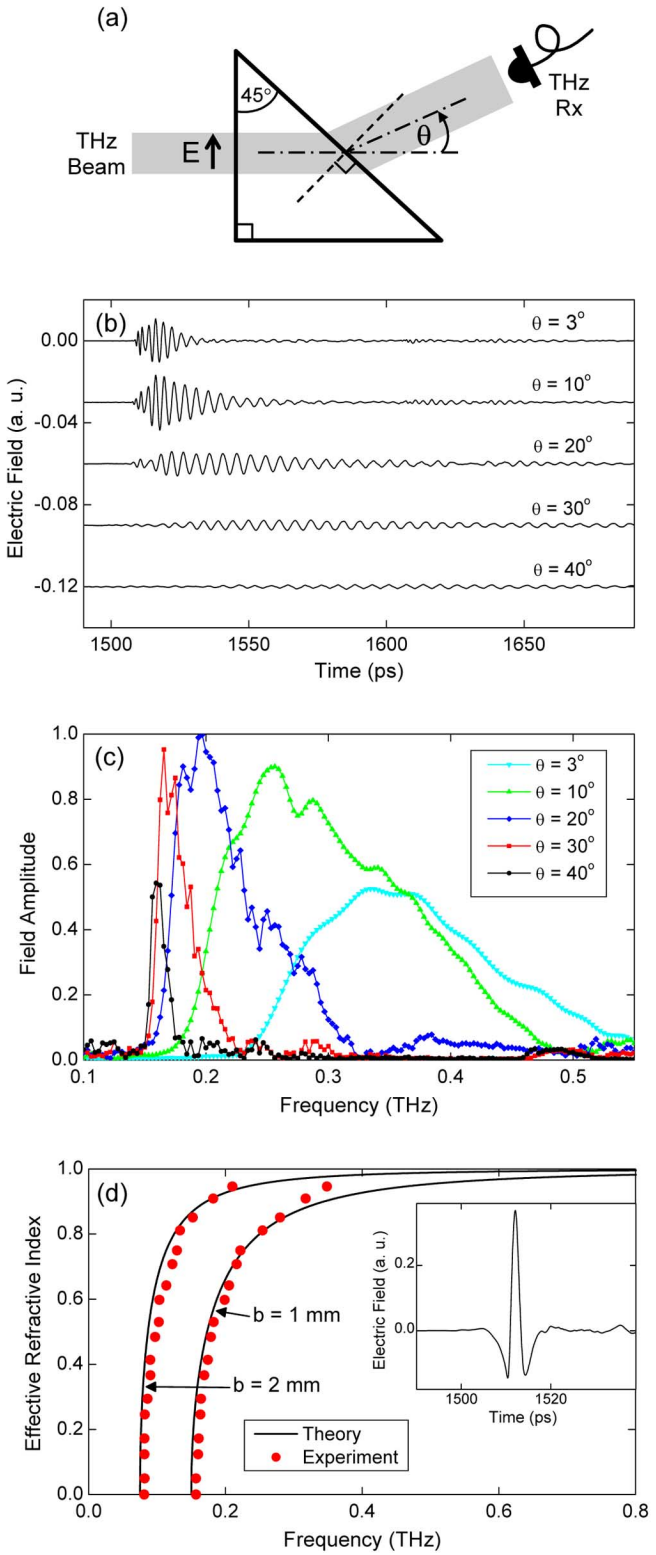

Fig. 1. (a) Schematic of the PPWG-prism. The width of the input face is 38.1 mm. (b) Terahertz signals detected at various Rx (angular) positions. (c) Corresponding amplitude spectra. (d) Comparison of the experimental and theoretical effective refractive index. The inset gives the input signal to the prism, which has frequency components varying from close to dc to about 1 THz.

TE_1-mode propagation [18], [19]. As the angle θ increases, we observe a decay in the high-frequency components and an enhancement in the low-frequency components. This dramatic *down shifting* is also evident in the amplitude spectra, where the spectral content evolves towards the low frequencies as θ increases from 0°, reaching frequencies near f_c at 45°. The finite size of the receiver's collecting aperture results in relatively broader spectra at low θ angles due to the more slowly varying index at higher frequencies.

Fig. 1(d) shows the experimentally derived refractive index (red dots in online version) compared to the theoretical curve based on (1) for $b = 1$ mm and 2 mm. In the experiment, the index values were derived using Snell's law for the respective θ values. The associated frequency values were derived using the center point of the ninetieth percentile level of each amplitude spectrum. This shows very good agreement between experiment and theory, where the slight shift of the experimental values towards the high-frequency end is due to the loss in signal content near the cutoff. This demonstration proves that the PPWG mimics a dielectric medium with $0 \leq n < 1$. Due to the dual-plate PPWG structure employed in this experiment (and the experiments that follow), the geometry of the artificial dielectric medium is limited to two dimensions (2-D). To extend this geometry to the third dimension (3-D), we can construct this structure using a *stacked set* of thin parallel metal plates [21]. However, it is impossible to achieve true 3-D behavior since there cannot be any propagation normal to the plates.

III. Total-Internal-Reflection Experiment

Since a wave entering the PPWG and propagating via the TE_1 mode travels from a high-index medium (free space, $n = 1$) to a low-index medium $(n < 1)$, one might expect to be able to observe TIR [26], or more specifically, total reflection, using this artificial dielectric medium. Based on Snell's law, the critical angle θ for TIR at the input face is given by

$$\sin\theta = n. \tag{2}$$

Substituting into (1), and simplifying, we get

$$f_{\mathrm{TIR}} = \frac{f_c}{\cos\theta} \tag{3}$$

where $0° \leq \theta < 90°$. Equation (3) suggests that a wave (with frequency f_{TIR}) entering the PPWG at the incidence angle of θ undergoes total reflection, and does not propagate into the PPWG. We note that when $\theta = 0°$ (normal incidence), $f_{\mathrm{TIR}} = f_c$; results in the self-consistent cutoff condition of the TE_1 mode. Therefore, the physical interpretation of this result is that as θ increases from normal incidence, the apparent cutoff shifts from f_c to higher frequencies. In other words, as θ increases, more and more frequencies reach the critical angle and are prohibited from entering the waveguide.

In order to test this experimentally, we used the PPWG configuration shown in Fig. 2(a). The PPWG was fabricated using two polished rectangular aluminum plates designed to provide a propagation length (for normal incidence) of 3.2 mm. This relatively short length was chosen to minimize the offset of the output beam compared to the input (the offset shown in Fig. 2(a) is exaggerated). The plate separation was chosen to be 1 mm. Similar to the first experiment, a beam of broadband terahertz pulses was focused to a 10-mm ($1/e$ amplitude) diameter and

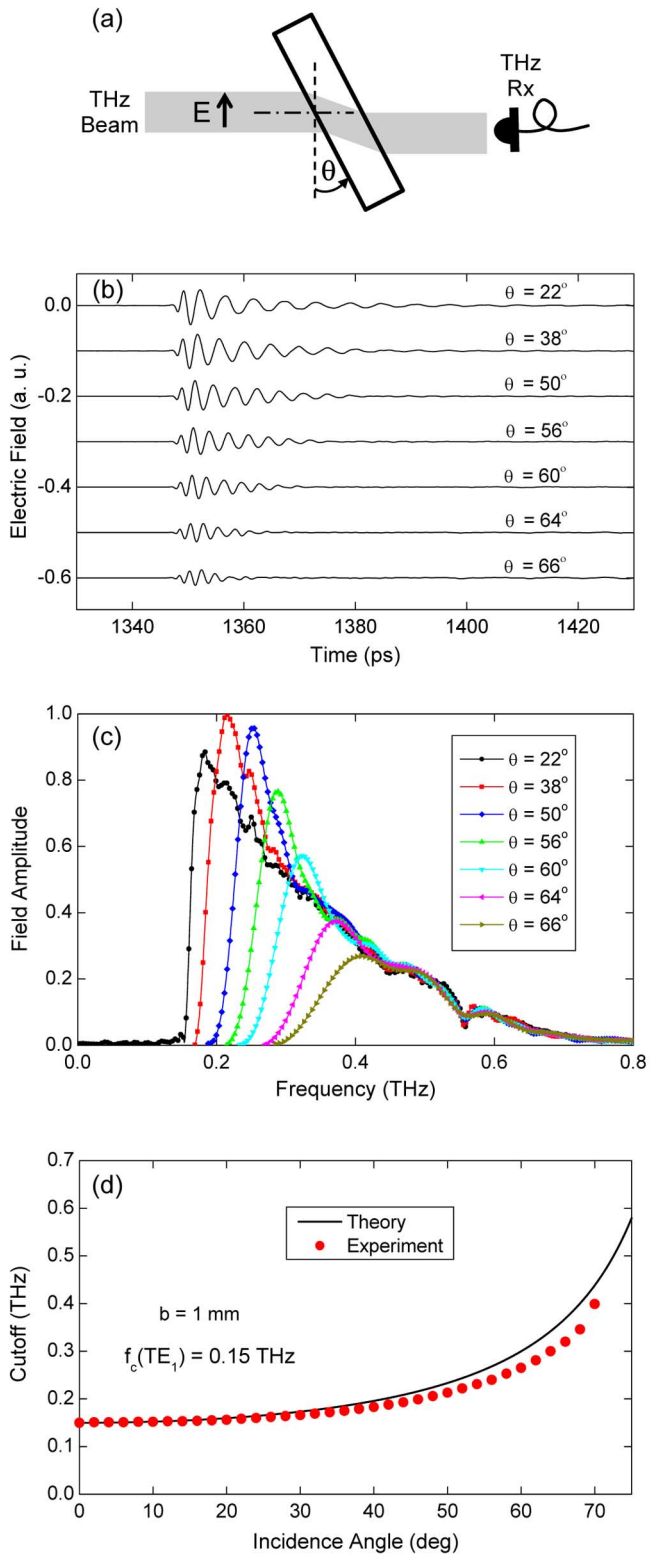

Fig. 2. (a) Schematic for the total-internal-reflection demonstration. The width of the input face is 31.8 mm. (b) Terahertz signals detected while rotating the PPWG with respect to the incident beam. (c) Corresponding amplitude spectra. (d) Comparison of the experimental and theoretical cutoff.

coupled into the waveguide with the electric field polarized parallel to the plate surfaces to excite the TE_1 mode. As shown in this figure, the PPWG was then rotated with respect to the input beam, and the propagated signal was detected at the output of the waveguide. Throughout the experiment, the receiver was fixed in place since the offset of the output beam was small.

The detected signals are shown in Fig. 2(b) with their corresponding amplitude spectra in Fig. 2(c). Unlike in the previous experiment, here we observe basically no change in the high-frequency components of the signal, but with a very dramatic *up shifting* of the cutoff as θ increases. Fig. 2(d) compares the theoretical (apparent) cutoff (for $b = 1$ mm) with the experimental values, which were derived using the twentieth percentile of the leading edge of each spectrum. The deviation of the experimental values (toward low frequencies) with increasing incidence angle is probably due to the leakage of low-frequency components since the input face of the waveguide experiences a diverging beam as the waveguide rotates. This low-frequency leakage increases with the incidence angle since the effective beam divergence experienced by the waveguide also increases. Nonetheless, this demonstration is clear evidence for total reflection in this artificial dielectric medium.

IV. Brewster's Effect Experiment

Next, we look at the possibility of demonstrating the Brewster's effect, a well-known optical phenomenon that results in total transmission (or no reflection) for p-polarized light traveling from one medium to another [26]. The angle at which this occurs, the Brewster's angle, is given by

$$\theta_B = \tan^{-1}\left(\frac{n_2}{n_1}\right) \tag{4}$$

where n_1 and n_2 are the refractive indices of the input and output media. Since the electric-field polarization of the TE_1 mode is similar to p-polarized light, we could expect to see the Brewster's effect for a TE_1-mode wave traveling from inside the PPWG to outside (free space, $n_2 = 1$). In this case, to achieve for example a $\theta_B = 60°$, we would need $n_1 = 0.577$, which should be possible based on the results shown in Fig. 1(d). In fact, for a plate separation of 1 mm, this should occur at a frequency of approximately 0.18 THz.

In order to test this experimentally, we used the configuration shown in Fig. 3(a). The PPWG-prism was fabricated using two polished aluminum plates shaped into identical equilateral triangles. As shown, the 1 cm-size terahertz beam enters the prism at the first air/PPWG interface at normal incidence, and reflects off of the second air/PPWG interface at an angle of 60° (while part of the energy escapes to free space), and then leaves the prism at the third interface at normal incidence. The detected signal at the output near the third interface is shown in Fig. 3(b), exhibiting a somewhat complicated structure. The corresponding amplitude spectrum is shown in Fig. 3(c) by the dots. Interestingly, the spectrum indicates a very clear *null* around 0.18 THz, signifying a zero reflection coefficient (at the second air/PPWG interface) due to the Brewster's condition. Fig. 3(c) also includes the magnitude of the theoretical reflection coefficient (red curve in online version) computed for the second interface using the measured value of $b = 0.992$ mm and 60° incidence. The theoretical null is in excellent agreement with the experimental one at a frequency of 0.185 THz. The inset shows the phase spectrum of the time signal in the vicinity of the null, indicating a

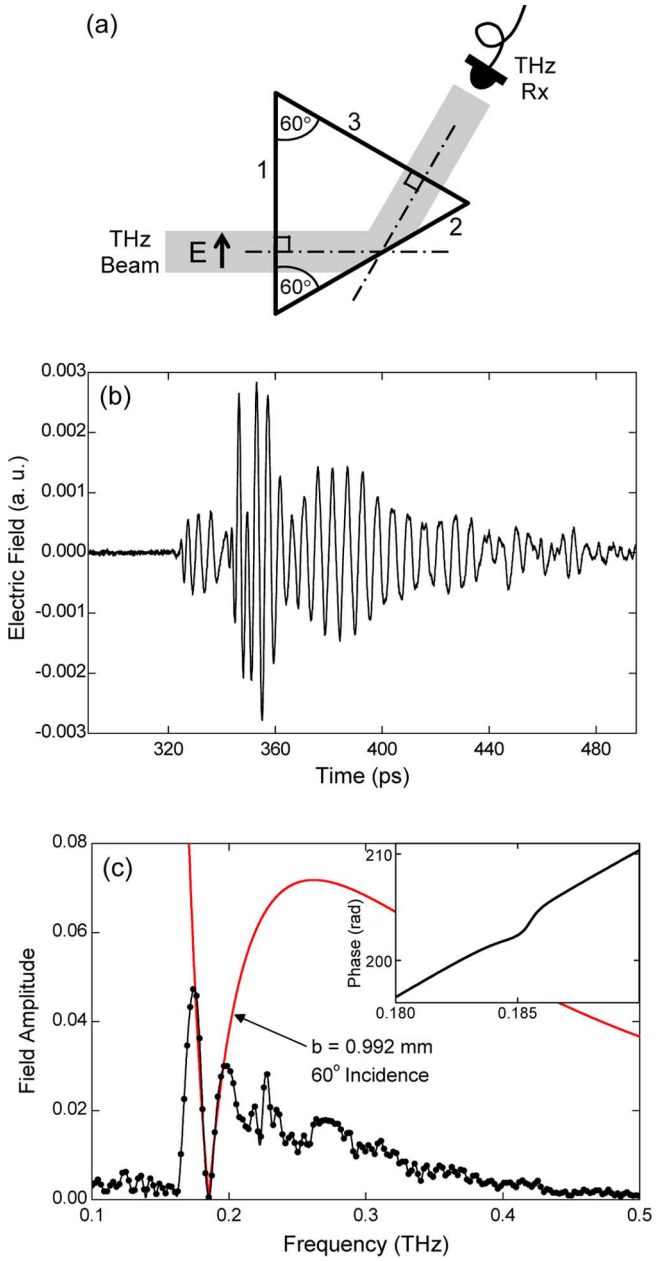

Fig. 3. (a) Schematic for the Brewster's effect demonstration. The width of the input face is 11.4 mm. (b) Terahertz signal reflected off of the second air/PPWG interface. (c) Corresponding amplitude spectrum compared to the theoretical refection coefficient (red curve in online version) indicating the null due to the Brewster's effect. The inset shows the corresponding phase spectrum near the null, indicating a phase jump.

clear phase jump. This corresponds to a 180° phase shift when the sign of the reflection coefficient changes from negative to positive.

V. PPWG-Lens Experiment

As a final demonstration, we construct a convergent PPWG-lens based on this artificial dielectric [see Fig. 4(a) and (b)]. Since the artificial dielectric medium has a refractive index less than that of free space, to achieve a positive lensing effect, one needs to use a concave geometry, rather than the usual convex geometry employed with conventional dielectrics. Therefore,

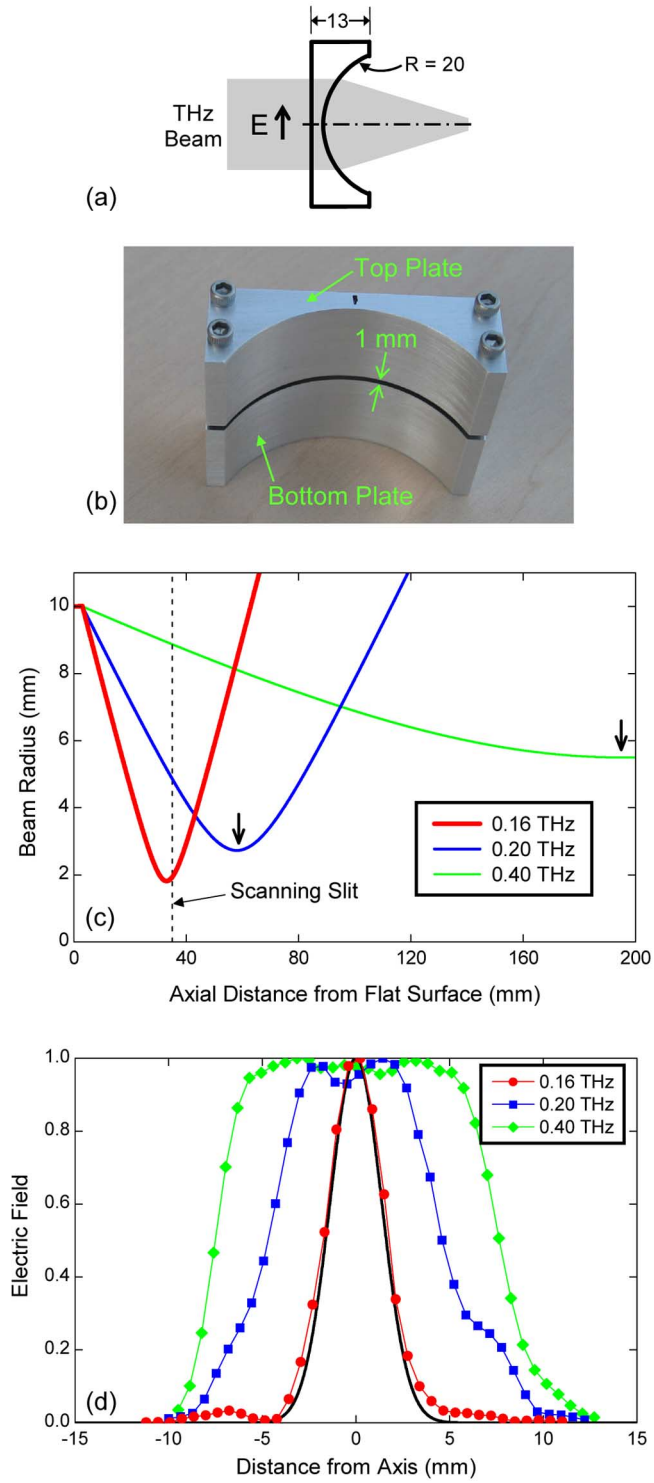

Fig. 4. (a) Schematic of the PPWG-lens. The width of the input face is 40 mm. Dimensions in millimeters. (b) Photograph of the fabricated device indicating the 1-mm gap between the two plates. (c) Gaussian beam calculation of the evolution of the output-beam radius for 0.16 THz (red in online version), 0.20 THz (blue in online version), and 0.40 THz (green in online version). The dashed line (35 mm away from the flat input surface) indicates the path of the slit. The vertical arrows indicate the foci. (d) Derived experimental electric field profiles at the 35-mm transverse plane. The solid black curve is the theoretical Gaussian profile for 0.16 THz.

the lens was designed with a plano-concave geometry, having a radius of curvature of 20 mm, and fabricated using two polished

aluminum plates with a 1-mm separation. The input terahertz beam was 20-mm ($1/e$ amplitude) diameter, and was reshaped to a line-focus at the input coupling face (to improve the coupling efficiency) using a Teflon plano-cylindrical lens.

As the terahertz beam propagates through the lens, it undergoes focusing only along one dimension, i.e., in the direction parallel to the (inside) plate surfaces, while the output beam diffracts in the perpendicular direction. Fig. 4(c) gives the calculated longitudinal Gaussian beam profile (evolution of the beam radius) after the beam propagates through the lens, for the frequencies of 0.16, 0.20, and 0.40 THz. Evidently, the focal length is highly frequency dependent, varying from about 35 mm at 0.16 THz (near cutoff) to about 200 mm at 0.40 THz. Furthermore, the focusing power is extremely strong at the low-frequency end, while it weakens towards the high-frequency end.

In order to map the transverse profile of the output beam, we scanned a 1-mm slit aperture 35 mm away from the flat face of the lens [dashed line in Fig. 4(c)] with the slit oriented perpendicular to the inside plate surfaces. The 35-mm transverse plane was chosen because this corresponded to approximately the tightest focus. Using a confocal lens arrangement at the output, the slit-plane was then imaged onto the terahertz receiver. After obtaining time-domain data for each slit position, these were Fourier transformed, and the amplitude components corresponding to the above three frequencies were extracted to map the frequency-dependent field profiles. These profiles are shown in Fig. 4(d), where the corresponding theoretical Gaussian profile at 0.16 THz (solid black curve) is also included for comparison. At 0.16 THz, the experimental $1/e$ full-width is 4.2 mm, whereas the theoretical Gaussian beam width is 3.9 mm. At 0.20 THz, the experimental full-width is 10.6 mm, whereas the theoretical width is 9.7 mm. At 0.40 THz, the experimental full-width is 16.1 mm, whereas the theoretical width is 17.7 mm. There is excellent agreement between experiment and theory at 0.16 THz. The discrepancy at higher frequencies is probably due to the fact that the input terahertz beam is not a perfect Gaussian, as assumed in the calculation. Nonetheless, this demonstrates that one can achieve a very strong focusing power at the low-frequency limit (near the cutoff) using this PPWG-lens. It is also interesting to note that after propagating through the lens, the low-frequency components concentrate near the optical axis, which is in contrast to a conventional lens, where it is the high frequencies that focus more tightly.

VI. Conclusion

In conclusion, we have demonstrated a 2-D artificial dielectric medium for the terahertz region by exploiting the characteristic frequency dependence in the phase velocity of the TE_1 mode of the PPWG. This artificial medium exhibits a plasma-like behavior having a frequency-dependent refractive index that varies between zero and unity. We use this dielectric medium to demonstrate the fundamental optical phenomena of total (internal) reflection and Brewster's effect. We also demonstrate a PPWG-lens with a strong focusing power suitable for the terahertz region. The PPWG-lens exhibits a focus and a focal length, which are both frequency dependent, an effect which can be exploited for multispectral imaging applications [27]. We can envision additional applications of this dielectric medium in frequency agile beam scanners, spatial filters, multiplexers, and invisibility cloaks. These results highlight the importance of this 2-D dielectric medium for fundamental research and technological applications.

References

[1] R. Mendis and D. Grischkowsky, "Undistorted guided-wave propagation of subpicosecond terahertz pulses," *Opt. Lett.*, vol. 26, pp. 846–848, Jun. 2001.

[2] R. Mendis and D. Grischkowsky, "THz interconnect with low loss and low group velocity dispersion," *IEEE Microw. Wireless Compon. Lett.*, vol. 11, no. 11, pp. 444–446, Nov. 2001.

[3] H. Cao, R. A. Linke, and A. Nahata, "Broadband generation of terahertz radiation in a waveguide," *Opt. Lett.*, vol. 29, pp. 1751–1753, Aug. 2004.

[4] S. Coleman and D. Grischkowsky, "Parallel plate THz transmitter," *Appl. Phys. Lett.*, vol. 84, pp. 654–656, Feb. 2004.

[5] R. Mendis, "Guided-wave THz time-domain spectroscopy of highly doped silicon using parallel-plate waveguides," *Electron. Lett.*, vol. 42, pp. 19–21, Jan. 2006.

[6] J. S. Melinger, N. Laman, S. S. Harsha, and D. Grischkowsky, "Line narrowing of terahertz vibrational modes for organic thin polycrystalline films within a parallel plate waveguide," *Appl. Phys. Lett.*, vol. 89, Dec. 2006, Art. ID 251110.

[7] N. Laman, S. S. Harsha, D. Grischkowsky, and J. S. Melinger, "High-resolution waveguide THz spectroscopy of biological molecules," *Biophys. J.*, vol. 94, pp. 1010–1020, Feb. 2008.

[8] J. Zhang and D. Grischkowsky, "Waveguide THz time-domain spectroscopy of nm water layers," *Opt. Lett.*, vol. 29, pp. 1617–1619, Jul. 2004.

[9] M. Nagel, M. Forst, and H. Kurz, "THz biosensing devices: Fundamentals and technology," *J. Phys., Condens. Matter.*, vol. 18, pp. S601–S618, Apr. 2006.

[10] M. M. Awad and R. A. Cheville, "Transmission terahertz waveguide-based imaging below the diffraction limit," *Appl. Phys. Lett.*, vol. 86, p. 221107, May 2005.

[11] D. G. Cooke and P. U. Jepsen, "Optical modulation of terahertz pulses in a parallel plate waveguide," *Opt. Exp.*, vol. 16, pp. 15123–15129, Sep. 2008.

[12] Z. Jian, J. Pearce, and D. M. Mittleman, "Defect modes in photonic crystal slabs studied using terahertz time-domain spectroscopy," *Opt. Lett.*, vol. 29, pp. 2067–2069, Sep. 2004.

[13] Y. Zhao and D. Grischkowsky, "2-D terahertz metallic photonic crystals in parallel-plate waveguides," *IEEE Trans. Microw. Theory Tech.*, vol. 55, no. 4, pp. 656–663, Apr. 2007.

[14] A. L. Bingham and D. Grischkowsky, "High Q, one-dimensional terahertz photonic waveguides," *Appl. Phys. Lett.*, vol. 90, Feb. 2007, Art. ID 091105.

[15] T. Prasad, V. L. Colvin, Z. Jian, and D. M. Mittleman, "Superprism effect in a metal-clad terahertz photonic crystal slab," *Opt. Lett.*, vol. 32, pp. 683–685, Mar. 2007.

[16] S. S. Harsha, N. Laman, and D. Grischkowsky, "High-Q terahertz bragg resonances within a metal parallel plate waveguide," *Appl. Phys. Lett.*, vol. 94, Mar. 2009, Art. ID 091118.

[17] B. G. Ghamsari and A. H. Majedi, "Terahertz transmission lines based on surface waves in plasmonic waveguides," *J. Appl. Phys.*, vol. 104, Oct. 2008, Art. ID 083108.

[18] R. Mendis and D. M. Mittleman, "An investrigation of the lowest-order transverse-electric (TE_1) mode of the parallel-plate waveguide for THz pulse propagation," *J. Opt. Soc. Amer. B, Opt. Phys.*, vol. 26, pp. A6–A13, Sep. 2009.

[19] R. Mendis and D. M. Mittleman, "Comparison of the lowest-order transverse-electric (TE_1) and transverse-magnetic (TEM) modes of the parallel-plate waveguide for terahertz pulse applications," *Opt. Exp.*, vol. 17, pp. 14839–14850, Aug. 2009.

[20] N. Marcuvitz, *Waveguide Handbook*. London, U.K.: Peregrinus, 1993.

[21] W. E. Kock, "Metal-lens antennas," *Proc. IRE*, vol. 34, pp. 828–836, Nov. 1946.

[22] J. Brown, "Artificial dielectrics having refractive indices less than unity," *Proc. IEEE* , vol. 100, no. 62R, pp. 51–62, May 1953, (monograph).

[23] J. S. Seeley and J. Brown, "The use of artificial dielectrics in a beam-scanning prism," *Proc. IEEE*, vol. 105C, no. 11, pp. 93–102, Nov. 1958, Paper 2735R.
[24] W. Rotman, "Plasma simulation by artificial dielectrics and parallel-plate media," *IRE Trans. Antennas Propag.*, vol. AP-10, no. 1, pp. 82–95, Jan. 1962.
[25] A. C. Brown, "Pattern shaping with a metal plate lens," *IEEE Trans. Antennas Propag.*, vol. AP-28, no. 4, pp. 564–568, Jul. 1980.
[26] E. Hecht, *Optics*. San Francisco, CA: Addison-Wesley, 2002.
[27] S. Wang, T. Yuan, E. D. Walsby, R. J. Blaikie, S. M. Durbin, D. R. S. Cumming, J. Xu, and X. -C. Zhang, "Characterization of T-ray binary lenses," *Opt. Lett.*, vol. 27, pp. 1183–1185, Jul. 2002.

Rajind Mendis (M'05) received the B.S. degree in electronic and telecommunication engineering from the University of Moratuwa, Moratuwa, Sri Lanka, in 1995, and the Ph.D. degree in electrical engineering from Oklahoma State University, Stillwater, in 2001.

From 2002 to 2004, he was with the Institute of High-Frequency Engineering, Technical University of Darmstadt, Darmstadt, Germany. From 2004 to 2007, he was with the Faculty of Engineering, University of Wollongong, Wollongong, N.S.W., Australia. Since 2007, he has been with the Department of Electrical and Computer Engineering, Rice University, Houston, TX. His research interests are in terahertz science and technology with a special emphasis on terahertz waveguides.

Dr. Mendis is a Senior Member of the Optical Society of America (OSA).

Daniel M. Mittleman (M'02–SM'07) was born in Berkeley, CA, in 1966. He received the B.S. degree in physics from the Massachusetts Institute of Technology (MIT), Cambridge, in 1988, and the M.S. and Ph.D. degrees in physics from the University of California at Berkeley, in 1990 and 1994, respectively.

He spent two years as a Post-Doctoral Member of the Technical Staff with Bell Laboratories, where he was involved in the development of terahertz "T-ray" imaging. In 1996, he joined the faculty of the Department of Electrical and Computer Engineering, Rice University, Houston, TX, where he is currently a Professor. His research involves ultrafast opto-electronic generation of terahertz radiation and its applications for spectroscopy, sensing, and imaging. He is also active in the study of new terahertz techniques, devices, and systems.

Prof. Mittleman is a Fellow of the Optical Society of America (OSA). He is a member of the American Physical Society and the IEEE Photonics Society.